Plant Communications
Research article

CellPress
Partner Journal

MoLrp1-mediated signaling induces nuclear accumulation of MoMsn2 to facilitate fatty acid oxidation for infectious growth of the rice blast fungus

Ting Zhang[1,2], Xingyu Wang[1,2], Xue Li[1,2], Ya-Nan Li[1,2], Yuhe Li[1,2], Shuang Wu[1,2], Lele Xu[1,2], Ruiwen Zhou[1,2], Jing Yang[1,2], Guotian Li[3], Xinyu Liu[1,2], Xiaobo Zheng[1,2], Zhengguang Zhang[1,2] and Haifeng Zhang[1,2,*]

[1]Department of Plant Pathology, College of Plant Protection, Nanjing Agricultural University, and Key Laboratory of Integrated Management of Crop Diseases and Pests, Ministry of Education, Nanjing, China

[2]The Key Laboratory of Plant Immunity, Nanjing Agricultural University, Nanjing, China

[3]State Key Laboratory of Agricultural Microbiology, Hubei Hongshan Laboratory, the Provincial Key Laboratory of Plant Pathology of Hubei Province, College of Plant Science & Technology, Huazhong Agricultural University, Wuhan, China

***Correspondence: Haifeng Zhang (hfzhang@njau.edu.cn)**

https://doi.org/10.1016/j.xplc.2023.100561

ABSTRACT

Fatty acid β-oxidation is critical for fatty acid degradation and cellular development. In the rice blast fungus *Magnaporthe oryzae*, fatty acid β-oxidation is reported to be important mainly for turgor generation in the appressorium. However, the role of fatty acid β-oxidation during invasive hyphal growth is rarely documented. We demonstrated that blocking peroxisomal fatty acid β-oxidation impaired lipid droplet (LD) degradation and infectious growth of *M. oryzae*. We found that the key regulator of pathogenesis, MoMsn2, which we identified previously, is involved in fatty acid β-oxidation by targeting *MoDCI1* (encoding dienoyl-coenzyme A [CoA] isomerase), which is also important for LD degradation and infectious growth. Cytological observations revealed that MoMsn2 accumulated from the cytosol to the nucleus during early infection or upon treatment with oleate. We determined that the low-density lipoprotein receptor-related protein MoLrp1, which is also involved in fatty acid β-oxidation and infectious growth, plays a critical role in the accumulation of MoMsn2 from the cytosol to the nucleus by activating the cyclic AMP signaling pathway. Our results provide new insights into the importance of fatty acid oxidation during invasive hyphal growth, which is modulated by MoMsn2 and its related signaling pathways in *M. oryzae*.

Key words: transcription factor MoMsn2, target gene, fatty acid β-oxidation, cAMP signaling, infectious growth

Zhang T., Wang X., Li X., Li Y.-N., Li Y., Wu S., Xu L., Zhou R., Yang J., Li G., Liu X., Zheng X., Zhang Z., and Zhang H. (2023). MoLrp1-mediated signaling induces nuclear accumulation of MoMsn2 to facilitate fatty acid oxidation for infectious growth of the rice blast fungus. Plant Comm. **4**, 100561.

INTRODUCTION

Fatty acids and their coenzyme A (CoA) esters play multiple roles in cellular processes as components of cellular lipids, carbon storage compounds in triacylglycerols, regulators of enzymes and membrane channels, ligands for nuclear receptors, and signaling molecules (Poirier et al., 2006; Aliyu et al., 2019). During an energy shortage, fatty acids released from lipid droplets (LDs) through lipolysis or lipophagy are used by mitochondria or peroxisomes for energy production via β-oxidation and the citric acid cycle (Olzmann and Carvalho, 2019). Although fatty acid β-oxidation is important for the maintenance of cellular fatty acid homeostasis, excess free fatty acids are toxic to cells (Rajvanshi et al., 2017; Olzmann and Carvalho, 2019). β-Oxidation is the principal means by which fatty acids are metabolized in cells. The mechanism of β-oxidation involves a set of four consecutive reactions catalyzed by four major enzymes of fatty acid oxidation, along with several other enzymes involved in degradation of

Published by the Plant Communications Shanghai Editorial Office in association with Cell Press, an imprint of Elsevier Inc., on behalf of CSPB and CEMPS, CAS.

unsaturated fatty acids (Wang et al., 2007). In yeasts and plants, the peroxisome is the sole site of fatty acid metabolism; by contrast, in other eukaryotes, including filamentous fungi, fatty acid metabolism also occurs in mitochondria (Hiltunen et al., 2003). *Magnaporthe oryzae*, the causative agent of the most destructive disease of cultivated rice worldwide, is a typical hemibiotrophic fungal pathogen (Ren and Schulz, 2003; Fatima and Senthil-Kumar, 2015; Abdul et al., 2018; Aliyu et al., 2019). Studies in *M. oryzae* have addressed the role of β-oxidation by focusing on peroxisome or mitochondrion biogenesis, the functions of multi-functional enzymes, and the contribution of β-oxidation to intracellular fatty acid metabolism (Wang et al., 2007; Patkar et al., 2012; Abdul et al., 2018; Aliyu et al., 2019). Strains defective in β-oxidation and peroxisome or mitochondrion biogenesis are impaired in appressorium development and infection (Hiltunen et al., 2003; Poirier et al., 2006; Goh et al., 2011; Fernandez et al., 2012; Wang et al., 2015; Deng et al., 2016; Abdul et al., 2018; Aliyu et al., 2019).

LDs, as cellular storage organelles, are highly dynamic and play a central role in lipid and energy homeostasis; they are composed of triacylglycerols (TAGs) and steryl esters in fungi (Graef, 2018; Jarc and Petan, 2019; Olzmann and Carvalho, 2019). LDs are thought to serve multiple functions within the cell: as a fuel involved in metabolic processes and membrane biosynthesis, as protein modifiers and signaling molecules, and as scavengers that protect against lipotoxicity by sequestering fatty acids (Kohlwein et al., 2013; Olzmann and Carvalho, 2019; Monson et al., 2021). Lipotoxicity is a pathophysiological process triggered by lipid overload that leads to organ dysfunction and cell death and is intimately linked to lipid-associated diseases such as cardiac dysfunction, cancer, and metabolic syndrome (Chang et al., 2015; Rockenfeller et al., 2018; Rockenfeller and Gourlay, 2018). Importantly, LD biogenesis and degradation are tightly coupled to cellular metabolism and are critical for buffering the levels of toxic lipid species (Olzmann and Carvalho, 2019). Inhibition of target of rapamycin in the *Fusarium* head blight fungus by rapamycin induces LD biogenesis through the FgPpg1/Sit4 signaling branch, leading to serious defects in vegetative growth, sexual development, and virulence (Liu et al., 2019). On the other hand, blocking autophagy inhibits LD degradation and causes an abnormal accumulation of LDs (Zienkiewicz and Zienkiewicz, 2020; Fu et al., 2021). Likewise, blocking fatty acid β-oxidation also causes abnormal LD accumulation (Rockenfeller and Gourlay, 2018; Jarc and Petan, 2019; Olzmann and Carvalho, 2019). Knockdown of the key peroxisomal fatty acid β-oxidation enzyme acyl-CoA oxidase 1 as well as treatment with the peroxisomal fatty acid β-oxidation inhibitor thioridazine specifically suppresses the oxidative respiration of persister cells and significantly impairs the hydrolysis of LDs (Shen et al., 2020). In mammalian cells, cyclic AMP (cAMP) signaling also regulates lipid metabolism, and inhibition of adenylate cyclase activity hinders cAMP synthesis and decreases lipolysis (Choi et al., 2006; Ravnskjaer et al., 2016). In response to elevated cAMP levels, several key regulators of lipolysis are activated, such as adipocyte-specific triglyceride lipase and the LD-associated protein perilipin (Brasaemle et al., 2009; Pagnon et al., 2012; Ravnskjaer et al., 2016). In summary, dysregulation of LD formation and/or degradation has been implicated in a wide variety of human and plant diseases (Greenberg et al., 2011; Liu et al., 2019; Shen et al., 2020; Wu et al., 2020).

LDs are dynamically synthesized and broken down in response to cellular and environmental signals (Petan et al., 2018; Jarc and Petan, 2019). Their accumulation is induced in cells exposed to excess amounts of lipids, nutrient stress, and various other conditions characterized by energetic and redox imbalances (Walther and Farese, 2012; Jarc and Petan, 2019). Response to environmental signals or stress requires a complex network of sensing and signal transduction mechanisms that include transcriptional regulation of genes (Rajvanshi et al., 2017). We found previously that the transcription factor (TF) MoMsn2 regulates the expression of a series of downstream genes and controls vegetative growth, conidiogenesis, cell wall integrity, stress response, mitochondrial morphology, and pathogenicity. Chromatin immunoprecipitation sequencing data revealed that MoMsn2 targets several genes involved in the β-oxidation pathway and likely plays a role in fatty acid metabolism (Zhang et al., 2014; Xiao et al., 2021). In this study, we demonstrate that MoMsn2 is involved in fatty acid β-oxidation by directly regulating its target gene *MoDCI1*, which encodes a dienoyl-CoA isomerase, and that MoMsn2 accumulates from the cytosol to the nucleus to promote fatty acid degradation, thereby facilitating invasive hyphal growth during the early infection stage. Further investigation revealed that the cAMP signaling pathway activated by MoLrp1 is required for accumulation of cytosolic MoMsn2 in the nucleus. Deletion of *MoLRP1*, *MoMSN2*, or *MoDCI1* or treatment with the peroxisomal fatty acid β-oxidation inhibitor thioridazine eventually leads to excessive accumulation of LDs and restricted infectious growth in rice. Our findings provide novel insights into the metabolic network that underlies fatty acid β-oxidation in *M. oryzae* during infection.

RESULTS

Impairment of peroxisomal fatty acid β-oxidation restricts infectious growth of *M. oryzae*

To investigate the relationship between fatty acid β-oxidation and pathogenicity of *M. oryzae*, we first evaluated the pathogenicity of the wild type Guy11 after treatment with the peroxisomal fatty acid β-oxidation inhibitor thioridazine (Thi) and found that it was unable to induce the defense response of rice (Supplemental Figure 1). Conidia treated with Thi caused fewer and smaller lesions with restricted invasive hyphal growth on rice compared with the untreated control (Figure 1A–1C). Because blocking fatty acid β-oxidation also causes abnormal LD accumulation (Rockenfeller and Gourlay, 2018; Jarc and Petan, 2019; Olzmann and Carvalho, 2019), we then asked whether such decreased virulence was associated with dysregulation of LD degradation by examining the quantity of LDs in the invasive hyphae. The number of LDs was significantly higher in the Thi treatment compared with the control (Figure 1D and 1E). We next analyzed the content of free fatty acids and the quantity of LDs using BODIPY 493/503, which is often used as a dye for lipid staining (Liu et al., 2019). We found that the content of free fatty acids and the number of LDs were clearly higher under Thi treatment (Figure 1F–1H). These findings suggest that peroxisomal fatty acid β-oxidation is critical for LD degradation and infectious growth of *M. oryzae*.

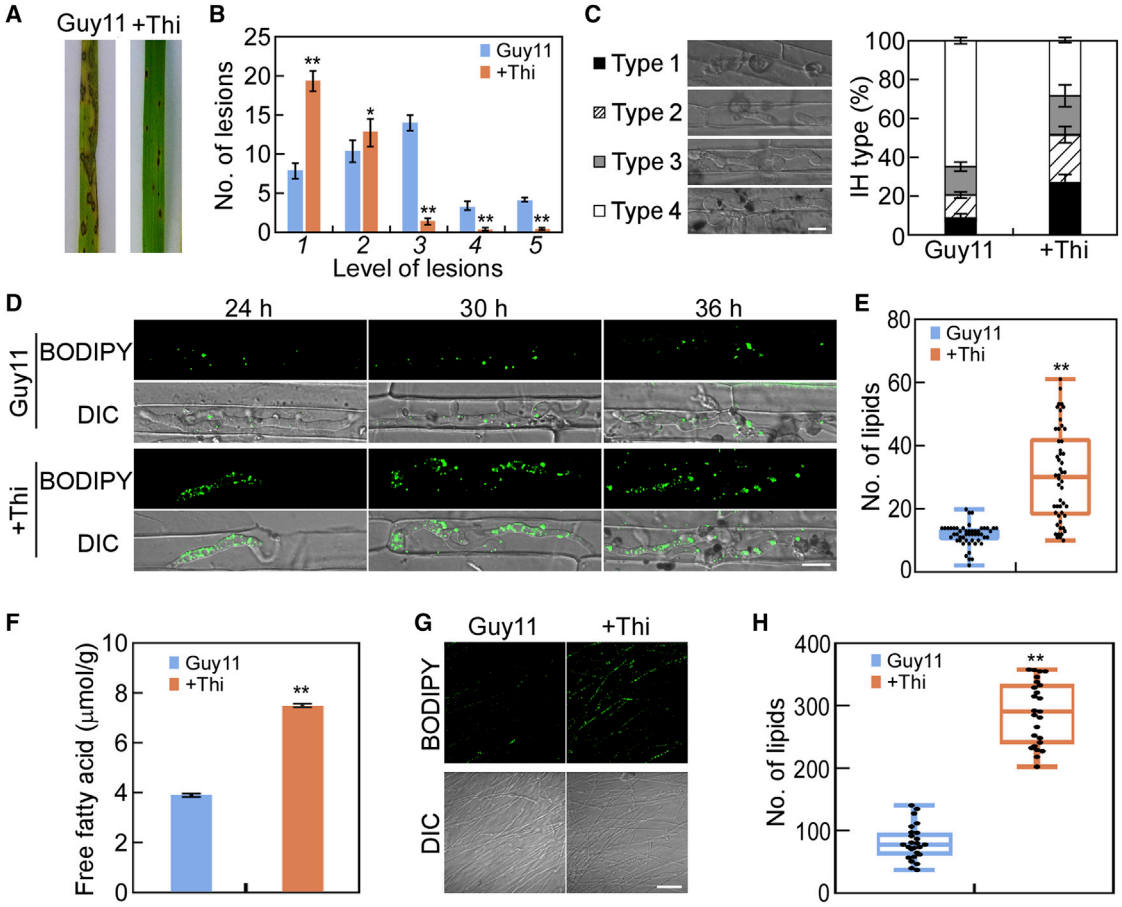

Figure 1. Impairment of peroxisomal fatty acid β-oxidation restricts infectious growth of *M. oryzae*.

(A) Pathogenicity assay. Conidial suspensions of wild-type Guy11 treated with or without thioridazine (Thi) were sprayed onto susceptible rice seedlings, which were photographed 5 days after incubation (dai). The final concentration of Thi was 0.001 mg/ml.

(B) Quantification of lesion types at 5 dai (1, pinhead-sized brown specks; 2, 1.5-mm brown spots; 3, 2- to 3-mm gray spots with brown margins; 4, many elliptical gray spots longer than 3 mm; 5, coalesced lesions). The number of lesions was counted within an area of 4 cm^2 on rice leaves. Error bars are SDs of three biological replicates, and asterisks indicate significant differences by two-tailed Student's *t*-test at $*p < 0.05$ and $**p < 0.01$.

(C) Conidial suspensions treated with or without Thi were injected into detached rice sheaths, and we statistically analyzed the percentage of invasive hypha (IH) types (type 1, no penetration; type 2, with penetration peg; type 3, with a single invasive hypha; type 4, with extensive hyphal growth) at 32 h post inoculation (hpi). Error bars are SDs of three biological replicates. Statistical analysis was performed by two-tailed Student's *t*-test. Scale bar, 20 μm.

(D) LDs were examined in Guy11 treated with or without Thi in IHs stained with BODIPY 493/503. Scale bar, 20 μm.

(E) Quantitative analysis of LDs in IHs of Guy11 treated with or without Thi. Fluorescence images were taken in 1×10^4 μm^2 from 50 fields of view in each strain using ImageJ, and the number of LDs is represented by a box-dot plot. Statistical analysis was performed by two-tailed Student's *t*-test using GraphPad Prism 8.0.1, and asterisks represent significant differences at $**p < 0.01$.

(F) Quantification of free fatty acids in Guy11 treated with or without Thi. Error bars are SDs of three biological replicates, and asterisks represent significant differences by two-tailed Student's *t*-test at $**p < 0.01$.

(G) LDs were examined in Guy11 treated with or without Thi in vegetative hyphae stained with BODIPY 493/503. Fluorescence images were obtained using the 3D reconstructed confocal z stack method with 20 photos. Scale bar, 100 μm.

(H) Quantitative analysis of LDs in Guy11 treated with or without Thi. Fluorescence images were taken in 1×10^4 μm^2 from 25 fields of view in each strain using ImageJ, and the number of LDs is represented by a box-dot plot. Statistical analysis was performed by two-tailed Student's *t*-test using GraphPad Prism 8.0.1, and asterisks represent significant differences at $**p < 0.01$.

MoMsn2 is involved in fatty acid oxidation

Our previous study demonstrated that the TF MoMsn2 plays pleiotropic roles in *M. oryzae* by modulating the expression of a series of genes (Zhang et al., 2014; Xiao et al., 2021). Our most recent chromatin immunoprecipitation sequencing data revealed that MoMsn2 likely plays a role in fatty acid metabolism by targeting several fatty acid β-oxidation-related genes, including *MGG_07019* (4-coumaryl-CoA ligase), *MoPOX1*, and *MoDCI1* (Xiao et al., 2021). Therefore, we first investigated whether MoMsn2 is involved in fatty acid oxidation. The wild type Guy11, the Δ*Momsn2* mutant, and the complemented transformant *MoMSN2-C* were inoculated onto minimal medium (MM) plates containing fatty acids with various chain lengths, including short-chain (butyrate), medium-chain (laurate), and long-chain (oleate [Ole] and olive oil [Oli]) fatty acids. After 7 days of incubation, the growth rate of the Δ*Momsn2* mutant was much lower than those of the wild type and the complemented transformant on Ole and

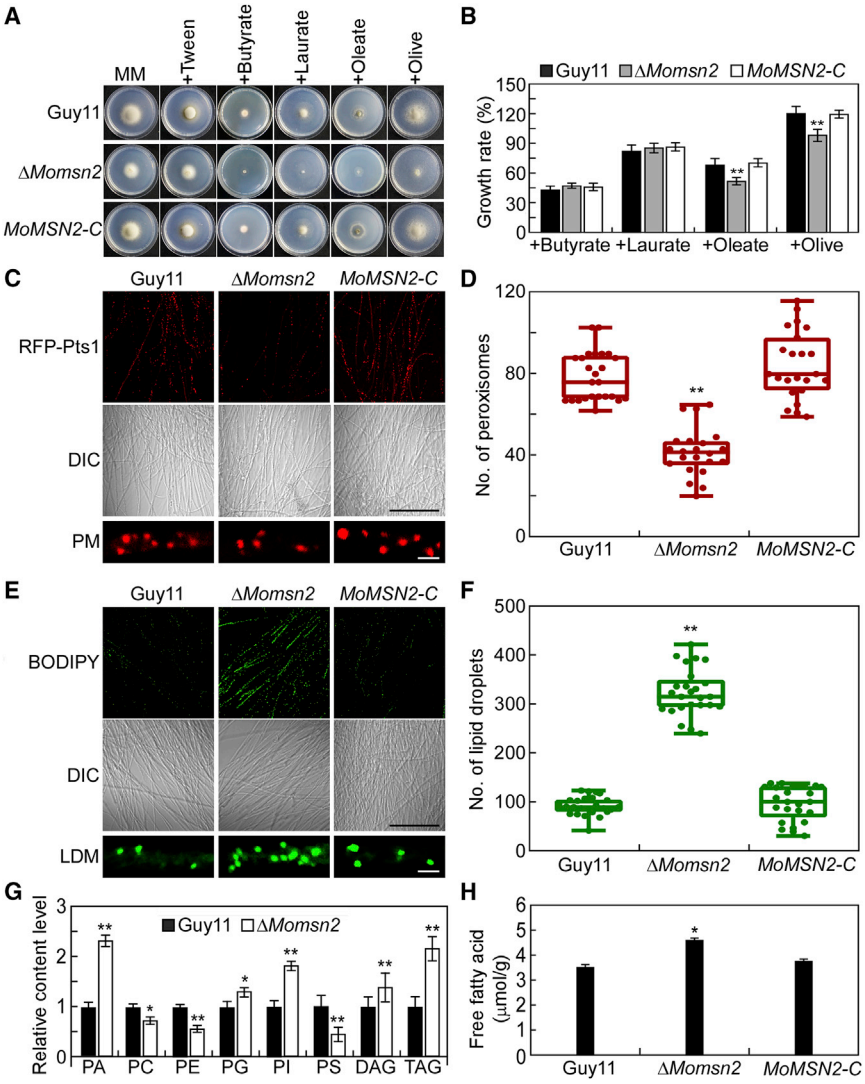

Figure 2. MoMsn2 is involved in fatty acid oxidation.

(A) The wild type Guy11, Δ*Momsn2* mutant, and complemented transformant *MoMSN2-C* were inoculated onto MM plates or MM with different fatty acids as carbon sources, cultured at 28°C for 7 days, and photographed.

(B) Statistical analysis of the growth rate of the indicated strains on different media. Error bars are SDs of three biological replicates, and asterisks represent significant differences by two-tailed Student's *t*-test at $^{**}p < 0.01$.

(C and D) The morphology and number of peroxisomes were examined and statistically analyzed in Guy11, Δ*Momsn2*, and *MoMSN2-C* strains expressing the RFP-Pts1 protein. Fluorescence images were taken using the 3D reconstructed confocal z stack method with 20 photos. Differential interference contrast images were taken under a confocal microscope. Quantitative analysis of peroxisomes was performed in 1×10^4 μm^2 from 25 fields of view in each strain using ImageJ (Media Cybernetics, Shanghai, China), and the number of peroxisomes is represented by a box-dot plot. Statistical analysis was performed by two-tailed Student's *t*-test using GraphPad Prism 8.0.1, and asterisks represents significant differences at $^{**}p < 0.01$. PM, peroxisome morphology. Black scale bar, 100 μm; white scale bar, 1 μm.

(E and F) The morphology and number of LDs were examined and statistically analyzed in Guy11, Δ*Momsn2*, and *MoMSN2-C* strains stained with BODIPY 493/503. Fluorescence images were taken using the 3D reconstructed confocal z stack method with 20 photos. Quantitative analysis of peroxisomes was performed in 1×10^4 μm^2 from 25 fields of view in each strain using ImageJ, and the number of peroxisomes is represented by a box-dot plot. Statistical analysis was performed by two-tailed Student's *t*-test using GraphPad Prism 8.0.1, and asterisks represent significant differences at $^{**}p < 0.01$. LDM, lipid droplet morphology. Black scale bar, 100 μm; white scale bar, 1 μm.

(G) High-performance liquid chromatography (HPLC)–mass spectrometry analysis of the lipid profiles of Guy11 and Δ*Momsn2*. DAG, diacylglycerol; PA, phosphatidic acid; PC, phosphatidylcholine; PE, phosphatidylethanolamine; PG, phosphatidylglycerol; PI, phosphatidylinositol; PS, phosphatidylserine; TAG, triacylglycerol. Means and SDs were calculated from four independent replicates. Asterisks indicate significant differences by two-tailed Student's *t*-test at $^{*}p < 0.05$ and $^{**}p < 0.01$.

(H) Quantification of free fatty acids in Guy11, Δ*Momsn2*, and *MoMSN2-C*. Error bars are SDs of three biological replicates, and asterisks represent significant differences by two-tailed Student's *t*-test at $^{*}p < 0.05$.

Oli plates but showed no apparent difference on butyrate and laurate plates (Figure 2A and 2B), suggesting that MoMsn2 plays a role in the oxidation of long-chain fatty acids.

The peroxisome is one of the main organelles in which fatty acid β-oxidation occurs in filamentous fungi (Wang et al., 2007). Therefore, we examined the morphology and quantity of peroxisomes in Guy11, Δ*Momsn2*, and *MoMSN2-C* expressing a red fluorescent protein (RFP)-Pts1 protein (RFP fused with peroxisomal targeting signal 1) (Zhong et al., 2016). Peroxisome morphology was not markedly altered in the mutant, but peroxisome number was significantly reduced (Figure 2C and 2D). LDs must be broken down into fatty acids, which are subsequently metabolized via β-oxidation during infection-related morphogenesis development of *M. oryzae* (Wang et al., 2007). Therefore, the morphology and quantity of LDs were also examined in hyphae of the mutant. The morphology of LDs was apparently unchanged, but their numbers were significantly higher in the mutant (Figure 2E and 2F). We next detected the lipid profile and the content of free fatty acids in the Δ*Momsn2* mutant. The lipidomic results showed that levels of phosphatidic acid, phosphatidylinositol (PI), diacylglycerol (DAG), and TAG (the main component of LDs) were much higher in the Δ*Momsn2* mutant than in the wild type Guy11, as was the content of free fatty acids (Figure 2G and 2H). These results suggest that MoMsn2 is important for fatty acid oxidation in *M. oryzae*.

MoMsn2 targets genes related to fatty acid β-oxidation

To explore the regulatory mechanism of MoMsn2 in fatty acid oxidation, we first validated the relationship between MoMsn2

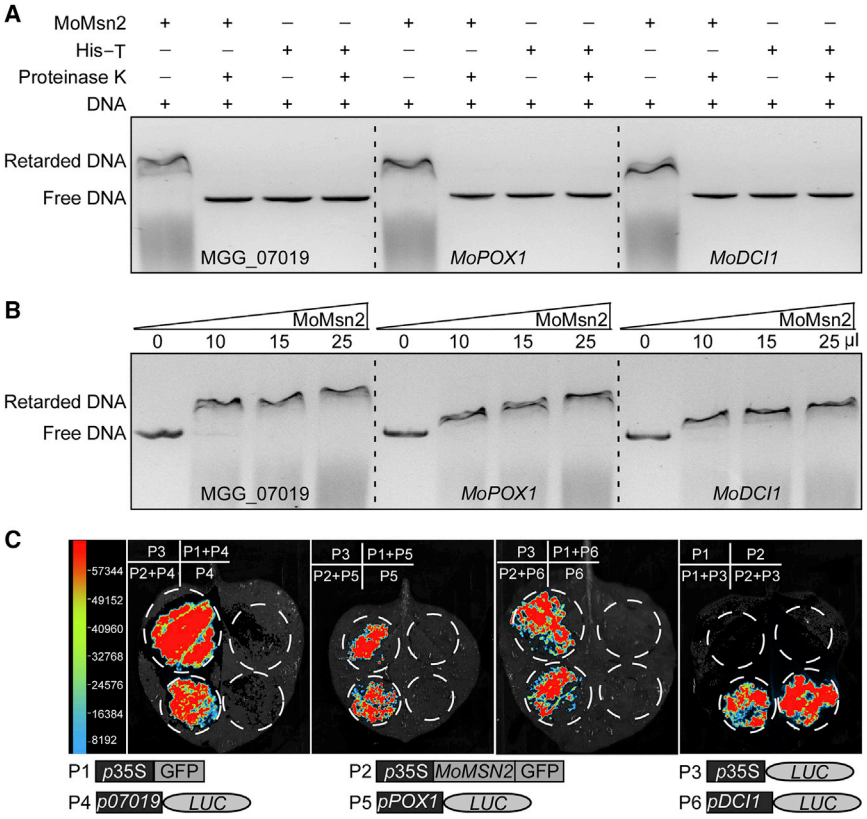

Figure 3. MoMsn2 targets fatty acid β-oxidation-related genes.

(A) EMSAs for binding of MoMsn2 protein with the putative promoter sequences of *MGG_07019*, *MoPOX1*, and *MoDCI1*. The 1500-bp DNA fragment of the putative promoter sequence of each gene was incubated in the absence or presence of purified MoMsn2 protein. pET-32a-His empty protein or proteinase K was added after incubation of MoMsn2 protein with the DNA fragment as a control. DNA–protein complexes were separated by 1.5% agarose gel electrophoresis and photographed. His-T, tag protein (hexahistidine and Trx) expressed by the empty vector pET-32a.

(B) EMSAs with increased amounts of MoMsn2 protein.

(C) Luciferase activity assay. The tested constructs were co-expressed or separately expressed in *N. benthamiana*. Luciferase activity was detected after 48 hpi. P1, negative control; P3, positive control.

and its potential target genes *MGG_07019, MoPOX1, and MoDCI1* using an electrophoretic mobility shift assay (EMSA). The MoMsn2 protein and protein expressed by an empty vector were confirmed by Coomassie brilliant blue staining before use in this assay (Supplemental Figure 2). The results showed that MoMsn2 binds to a putative promoter region 1500 bp upstream of the start codons of these three genes. MoMsn2–DNA complexes migrate more slowly than the DNA fragments alone in an agarose gel without proteinase K treatment (Figure 3A and 3B). We further confirmed the binding with a luciferase activity assay by transient expression in *Nicotiana benthamiana*. Strong luciferase activity was detected at the infiltration sites co-expressing *p35S-MoMSN2*-GFP/*p07019-LUC*, *p35S-MoMSN2*-GFP/*pPOX1-LUC*, and *p35S-MoMSN2*-GFP/*pDCI1-LUC*. High luciferase activity was detected when expressing single *p35S-LUC* or co-expressing *p35S-MoMSN2*-GFP/*p35S-LUC* or *p35S*-GFP/*p35S-LUC*. No luciferase activity was detected when expressing single *p35S*-GFP, *p35S-MoMSN2*-GFP, *p07019-LUC*, *pPOX1-LUC*, or *pDCI1-LUC* or co-expressing *p35S*-GFP/*p07019-LUC*, *p35S*-GFP/*pPOX1-LUC*, or *p35S*-GFP/*pDCI1-LUC* (Figure 3C). These results indicate that MoMsn2 targets genes related to fatty acid β-oxidation .

The target gene *MoDCI1* is involved in fatty acid oxidation and pathogenicity

To clarify the role of *MGG_07019*, *MoPOX1*, and *MoDCI1* in fatty acid oxidation and pathogenicity, we generated gene deletion mutants using a gene replacement strategy and Southern blot analysis (Supplemental Figure 3A–3C). In infection assays with the resulting mutants, only the Δ*Modci1* mutant, but not Δ*07019* or Δ*Mopox1*, showed reduced virulence (Supplemental Figure 3D–3F). We therefore focused on further studies with the Δ*Modci1* mutant. Phenotypic analysis revealed that the Δ*Modci1* mutant had vegetative growth, conidium production, and appressorium formation characteristics similar to those of the wild type Guy11 and the complemented transformant *MoDCI1-C* (Supplemental Table 1), but it showed defects in Ole and Oli oxidation (Figure 4A). The expression level of *MoDCI1* increased markedly in Guy11, but not in Δ*Momsn2*, under Ole and Oli treatment (Figure 4B), suggesting that induction of *MoDCI1* expression by long-chain fatty acids requires the upstream regulator MoMsn2. Deletion of *MoDCI1* resulted in fewer peroxisomes, more LDs, and higher levels of phosphatidylglycerol, PI, DAG, TAG, and free fatty acids compared with Guy11 and *MoDCI1-C*, mimicking the Δ*Momsn2* mutant (Figure 4C–4F). Pathogenicity analysis revealed that Δ*Modci1* generally caused smaller lesions with restricted growth of infectious hyphae (IHs), whereas Guy11 and *MoDCI1-C* caused typical coalescent lesions with extensive IHs. Similar results were obtained in infection assays with barley seedlings. The Δ*Modci1* mutant caused fewer blast lesions and green islands on barley leaves (Figure 4G–4I). We also overexpressed *MoDCI1* in the Δ*Momsn2* mutant and obtained the transformant Δ*Momsn2/DCI1*, which had an *MoDCI1* expression level 140-fold higher than that of the wild type, Guy11. Phenotypic analysis revealed that the growth rate on Ole plates, number of peroxisomes, and pathogenicity were partially restored in the Δ*Momsn2/DCI1* transformant (Supplemental Figure 4A–4F). Further examination of cellular localization revealed that MoDci1 was mainly distributed in the cytosol in vegetative hyphae and conidia but localized in peroxisomes in appressoria and IHs (Supplemental Figure 5A–5D). These results suggest that *MoDCI1* is a target of MoMsn2 in the regulation of fatty acid oxidation and infectious growth in *M. oryzae*.

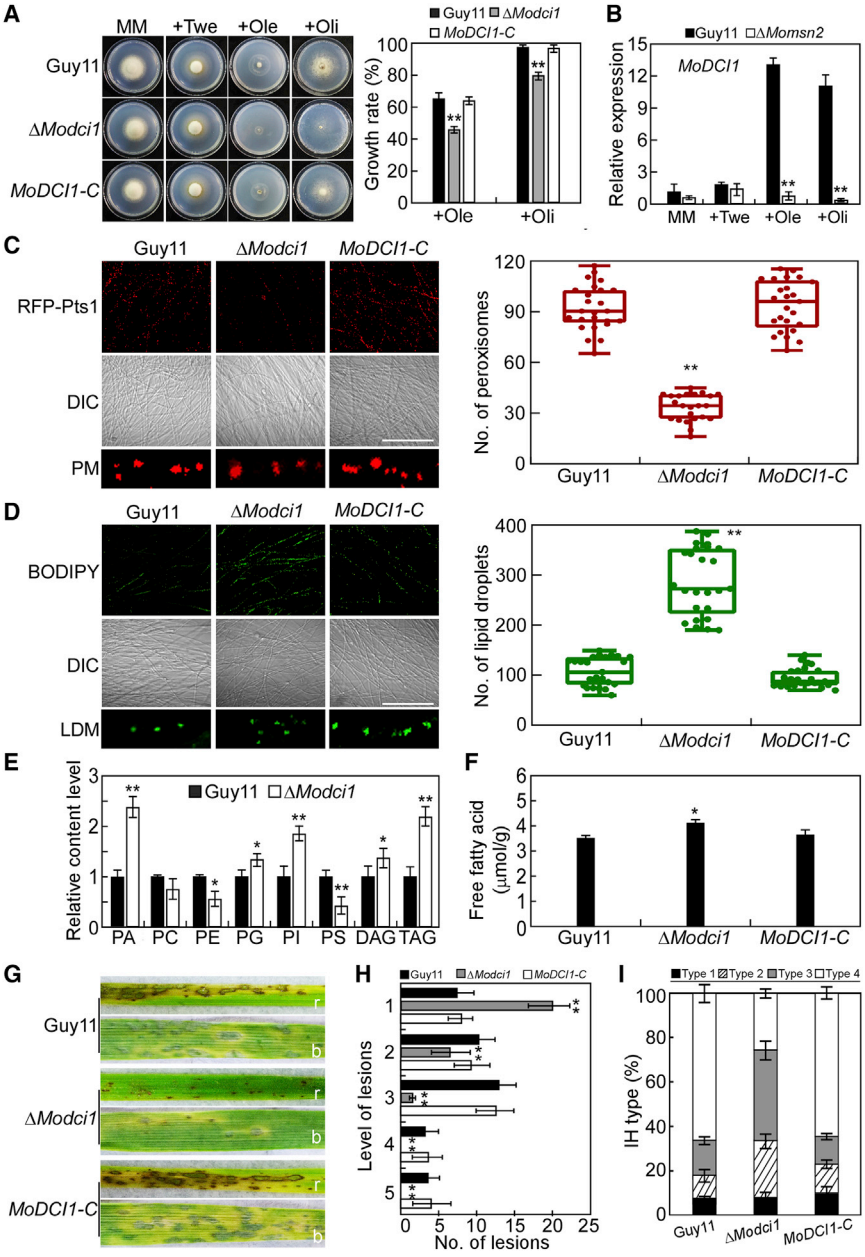

Figure 4. The target gene *MoDCI1* is involved in fatty acid oxidation and pathogenicity.

(A) Colony morphology and growth rate of the wild type Guy11, Δ*Modci1* mutant, and complemented transformant *MoDCI1-C* on MM or MM plates containing Tween 80 (Twe), oleate (Ole), and olive oil (Oli) as carbon sources. Error bars are SDs of three biological replicates, and asterisks represent significant differences by two-tailed Student's *t*-test at $^{**}p < 0.01$.

(B) qRT–PCR analyses of the expression levels of *MoDCI1* in Guy11 and Δ*Momsn2* in liquid MM with Glu, Twe, Ole, and Oli as carbon sources. Error bars are SDs of three biological replicates, and asterisks represent significant differences by two-tailed Student's *t*-test at $^{**}p < 0.01$.

(C) The morphology and the number of peroxisomes were examined and statistically analyzed in the indicated strains according to Figure 2C and 2D.

(D) The morphology and the number of LDs were examined and statistically analyzed in the indicated strains stained with BODIPY 493/503 according to Figure 2E and 2F.

(E) HPLC–mass spectrometry analysis of the lipid profiles of wild-type Guy11 and the Δ*Modci1* mutant. Means and SDs were calculated from four independent replicates. Asterisks indicate significant differences by two-tailed Student's *t*-test at $^{*}p < 0.05$ and $^{**}p < 0.01$.

(F) Quantification of free fatty acids in Guy11, Δ*Modci1*, and *MoDCI1-C*. Error bars are SDs of three biological replicates, and asterisks represent significant differences by two-tailed Student's *t*-test at $^{*}p < 0.05$.

(G) Pathogenicity assay. Conidial suspensions of Guy11, Δ*Modci1*, and *MoDCI1-C* were sprayed onto susceptible rice (r) and barley (b) seedlings and photographed at 5 and 4 dai, respectively.

(H) Quantification of lesion types at 5 dai. The number of lesions was counted within an area of 4 cm^2 on rice leaves. Error bars are SDs of three biological replicates, and asterisks indicate significant differences by two-tailed Student's *t*-test at $^{**}p < 0.01$.

(I) Conidial suspensions were injected into detached rice sheaths, and we statistically analyzed the percentages of IH types (refer to Figure 1C) at 32 hpi. Error bars are SDs of three biological replicates, and statistical analysis was performed by two-tailed Student's *t*-test.

Cytosolic MoMsn2 accumulates from the cytosol to the nucleus after treatment with long-chain fatty acids

The results above indicate that MoMsn2 functions in fatty acid oxidation by targeting *MoDCI1* in response to fatty acids. To determine how MoMsn2 is involved in this process, we examined the localization pattern of MoMsn2 under various fatty acid treatments. A strain co-expressing MoMsn2-GFP and H1-RFP (histone H1 protein with RFP) in the wild type Guy11 was generated. Fluorescence observations revealed that MoMsn2-GFP was localized in the cytosol and nucleus under normal conditions (MM-glucose) and accumulated from the cytosol to the nucleus under NaCl treatment, consistent with our previous findings (Zhang et al., 2014). MoMsn2-GFP also localized to the cytosol and nucleus upon treatment with butyrate or laurate, but it localized mainly in the nucleus in hyphae (65.4% ± 5.3%) and conidia (61.6% ± 8.5%) upon treatment with Ole (Figure 5A and Supplemental Figure 6A). To confirm these findings, we statistically analyzed the fluorescence signals of MoMsn2-GFP after normalizing with H1-RFP signals in each treatment and found that the ratios of the treatments with NaCl and Ole were much higher than those of the treatments with glucose, butyrate, and laurate in conidia (Supplemental Figure 6B). Western blot analysis revealed that the abundance of MoMsn2-GFP in the nucleus was higher in the NaCl and Ole treatments than in the glucose, butyrate, and laurate treatments (Supplemental Figure 6C). These results suggest that cytosolic

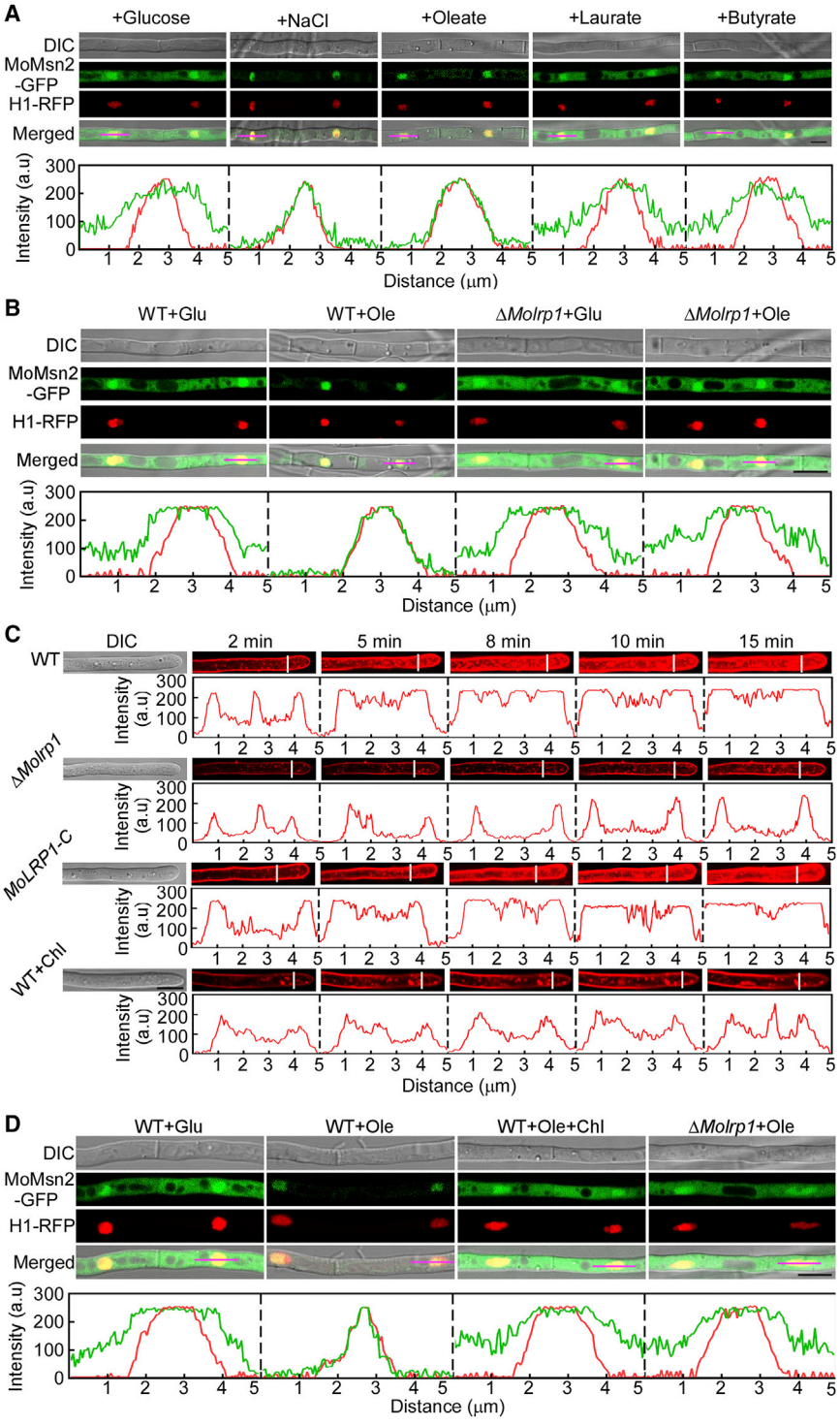

Figure 5. Endocytosis mediated by MoLrp1 is important for MoMsn2 accumulation from the cytosol to the nucleus under Ole treatment.

(A and B) Hyphae of wild-type Guy11 and the Δ*Molrp1* mutant co-expressing MoMsn2-GFP and H1-RFP proteins were observed under a confocal microscope after treatment with different fatty acids or NaCl for 10 or 30 min. NaCl treatment was used as a positive control. Insets highlight areas analyzed by line scan. The green line represents MoMsn2-GFP; the red line represents H1-RFP. Scale bar, 10 μm.

(C) Hyphae of Guy11, Δ*Molrp1*, and the complemented transformant *MoLRP1-C* with or without chlorpromazine (Chl) treatment were stained with FM4-64 and examined under a confocal microscope. Insets highlight areas analyzed by line scan. Scale bar, 10 μm.

(D) Hyphae of Guy11 and Δ*Molrp1* co-expressing MoMsn2-GFP and H1-RFP proteins were co-treated with Chl and Ole for 10 min and observed under a confocal microscope. Insets highlight areas analyzed by line scan. The green line represents MoMsn2-GFP; the red line represents H1-RFP. Scale bar, 10 μm.

MoMsn2 accumulates in the nucleus in response to long-chain fatty acids.

The cytosol-to-nucleus accumulation of MoMsn2 upon Ole treatment is defective in the Δ*Molrp1* mutant

The low-density lipoprotein receptor (LDLR) family is a group of endocytic receptors on the cell surface that bind and internalize extracellular ligands such as lipoproteins, exotoxins, and lipid-carrier complexes in mammalian cells (Willnow et al., 1999). LDLR-related protein 1 (LRP1) is a member of the LDLR family that has prominent functions in endocytosis, lipid metabolism, energy homeostasis, and signal transduction (Boucher and Herz, 2011). To investigate whether the translocation of MoMsn2 induced by fatty acids is involved in an LRP1-dependent signaling pathway, we identified MoLrp1 (MGG_04076), the *M. oryzae* homolog of mammalian LRP1, and generated the Δ*Molrp1* mutant (Supplemental Figure 7A and 7B). We obtained another strain by co-expressing MoMsn2-GFP and H1-RFP proteins in the Δ*Molrp1* mutant and examined the localization pattern of MoMsn2-GFP after treatment with glucose (as a control) or Ole. In the glucose treatment, the Δ*Molrp1* mutant showed no apparent differences in the localization pattern of MoMsn2-GFP, indicating that MoLrp1 does not regulate the localization of MoMsn2 under normal conditions. After treatment with Ole, cytosolic MoMsn2-GFP showed a defect in translocation from the cytosol to the nucleus and instead remained in the cytosol and nucleus of the mutant. By contrast, MoMsn2-GFP accumulated from the cytosol to the nucleus in hyphae and conidia of the wild-type strain upon treatment with Ole (Figure 5B and Supplemental Figure 8A). The statistical analysis of MoMsn2-GFP fluorescence signals after normalization with H1-RFP and the results of western blotting further supported our findings (Supplemental Figure 8B and 8C).

These results suggest that accumulation of cytosolic MoMsn2 in the nucleus in the presence of long-chain fatty acids is dependent on MoLrp1.

The role of MoLrp1 in endocytosis is important for MoMsn2 accumulation

MoLrp1 is essential for translocation of MoMsn2 in the presence of fatty acids, but the underlying mechanism remains unknown. Because mammalian LRP1 plays a role in endocytosis, we first evaluated endocytosis in the Δ*Molrp1* mutant by FM4-64 staining. The ability to take up N-(3-triethylammoniumpropyl)-4-(p-diethylamino-phenyl-hexatrienyl) pyridinium dibromide (FM4-64) was greatly reduced in vegetative hyphae of the mutant compared with those of the wild type Guy11 and the complemented transformant *MoLRP1-C*, even after incubation for 15 min (Figure 5C). We then examined the localization pattern of MoLrp1 in conidia and found that MoLrp1 was distributed mainly in the endoplasmic reticulum, Golgi complex, and endosomes on the basis of co-localization with MoLhs1 (an endoplasmic reticulum marker protein), MoSft2 (a Golgi marker protein), or FM4-64 stain (Supplemental Figure 9), respectively. These results were consistent with the function of LRP1 in mammalian cells (Bu et al., 1994). Mammalian LRP1 is a membrane protein confined to clathrin-coated pits (Bu et al., 1994; Lin et al., 2017), indicating that endocytosis mediated by MoLrp1 is likely to be clathrin dependent. We therefore examined endocytosis of wild-type Guy11 treated with chlorpromazine (Chl; an inhibitor of clathrin-mediated endocytosis; Rejman et al., 2005) and found that its ability to take up FM4-64 was similar to that of the Δ*Molrp1* mutant (Figure 5C). We further examined the dynamics of MoMsn2-GFP in Δ*Molrp1* and in Guy11 treated with Chl and found that MoMsn2-GFP showed a defect in accumulation from the cytosol to the nucleus in Δ*Molrp1* and Guy11+Chl under Ole treatment (Figure 5D). These results suggest that the role of MoLrp1 in endocytosis is important for MoMsn2 accumulation from the cytosol to the nucleus under Ole conditions.

MoLrp1 is important for fatty acid oxidation and pathogenicity

The results described above demonstrate that MoLrp1 is important for endocytosis and translocation of MoMsn2 in the presence of fatty acids, but whether it is involved in fatty acid oxidation or pathogenicity remains unclear. Therefore, we explored the biological role of MoLrp1 in *M. oryzae*. Phenotypic analysis revealed that vegetative growth, conidium production, appressorium formation, and appressorium turgor of Δ*Molrp1* showed no obvious differences from those of Guy11 and *MoLRP1-C* (Supplemental Table 2). Further analysis revealed that Δ*Molrp1* had a decreased growth rate on Ole and Oli plates, fewer peroxisomes, more LDs, and higher levels of PI, TAG, and free fatty acids compared with Guy11 and *MoLRP1-C* (Supplemental Figure 10A–10E). Pathogenicity analysis revealed that Δ*Molrp1* caused smaller lesions, whereas Guy11 and *MoLRP1-C* caused numerous coalescent lesions (Supplemental Figure 10F and 10G). Further examination revealed that over 70% of cells infected with Δ*Molrp1* showed type 1–3 IH growth compared with 35%–40% of cells infected with Guy11 or *MoLRP1-C*. By contrast, less than 30% of cells infected with Δ*Molrp1* showed type 4 IH growth compared with over 60% with Guy11 and *MoLRP1-C* (Supplemental Figure 10H). These results suggest that MoLrp1 functions in fatty acid oxidation and pathogenicity.

Intracellular cAMP level mediated by MoLrp1 is crucial for accumulation of MoMsn2 from the cytosol to the nucleus

Several studies have reported an important role of cAMP in lipolysis (Shepherd et al., 1981; Duncan et al., 2007; Ravnskjaer et al., 2016). Lipolysis in mature adipocytes induced by lactoferrin is regulated by controlling the activity of cAMP signaling pathways via LRP1 (Ikoma-Seki et al., 2015). To determine whether such MoLrp1-dependent lipid metabolism is associated with the cAMP pathway, we first measured the cAMP levels in Guy11 and Δ*Molrp1* with or without Ole treatment. The cAMP level was significantly lower in the Δ*Molrp1* mutant under normal conditions but much higher in wild-type Guy11 than in the control and mutant under Ole treatment (Figure 6A), indicating that MoLrp1 plays an important role in activating the cAMP signaling pathway in response to exogenous Ole. We next investigated the pathogenicity of the Δ*Molrp1* mutant with cAMP treatment and found that the pathogenicity defect of the mutant was greatly rescued (Figure 6B and 6C). We then investigated whether the cAMP signaling mediated by MoLrp1 is related to accumulation of MoMsn2. MoMsn2-GFP dynamics were examined in the wild-type strain and Δ*Molrp1* mutant treated with or without cAMP. Fluorescence observations revealed that MoMsn2-GFP accumulated from the cytosol to the nucleus upon treatment with cAMP or Ole in the wild-type strain, but this accumulation was compromised upon co-treatment with N-(cis-2-phenylcyclopentyl) azacyclotridecan-2-imine hydrochloride (MDL-12330A) (a type of adenylate cyclase inhibitor) and Ole. MoMsn2-GFP was localized in the cytosol and nucleus under normal conditions and under treatment with Ole in the Δ*Molrp1* mutant but accumulated from the cytosol to the nucleus upon treatment with cAMP (Figure 6D). These results suggest that the intracellular cAMP level mediated by MoLrp1 is crucial for accumulation of MoMsn2 from the cytosol to the nucleus.

MoMsn2 accumulates from the cytosol to the nucleus during the early infectious stage, relying on MoLrp1

To investigate whether MoMsn2 is involved in oxidation of fatty acids during infection, we first examined the localization pattern of MoMsn2 in early IHs. Accumulation of MoMsn2-GFP in the nucleus was observed in 84.7% of IHs in wild-type Guy11 compared with 41.3% of IHs in the Δ*Molrp1* mutant (Figure 6E and 6F). These results indicated that MoLrp1 is important for translocation of MoMsn2 to the nucleus during early infection. We further evaluated the expression of *MoLRP1* during infection and under Ole treatment and found that *MoLRP1* was highly expressed in IHs at 24 h post inoculation (hpi) and under Ole treatment. We also examined the expression of *MoDCI1* during infection and in the Δ*Molrp1* mutant under Ole treatment and found that *MoDCI1* expression was strongly induced in IHs at 24 hpi compared with vegetative hyphae. However, *MoDCI1* expression was much lower in the Δ*Molrp1* mutant than in the wild type when treated with Ole (Figure 6G and 6H). These results indicate that MoMsn2 accumulates from the cytosol to the nucleus, dependent on strong induction of

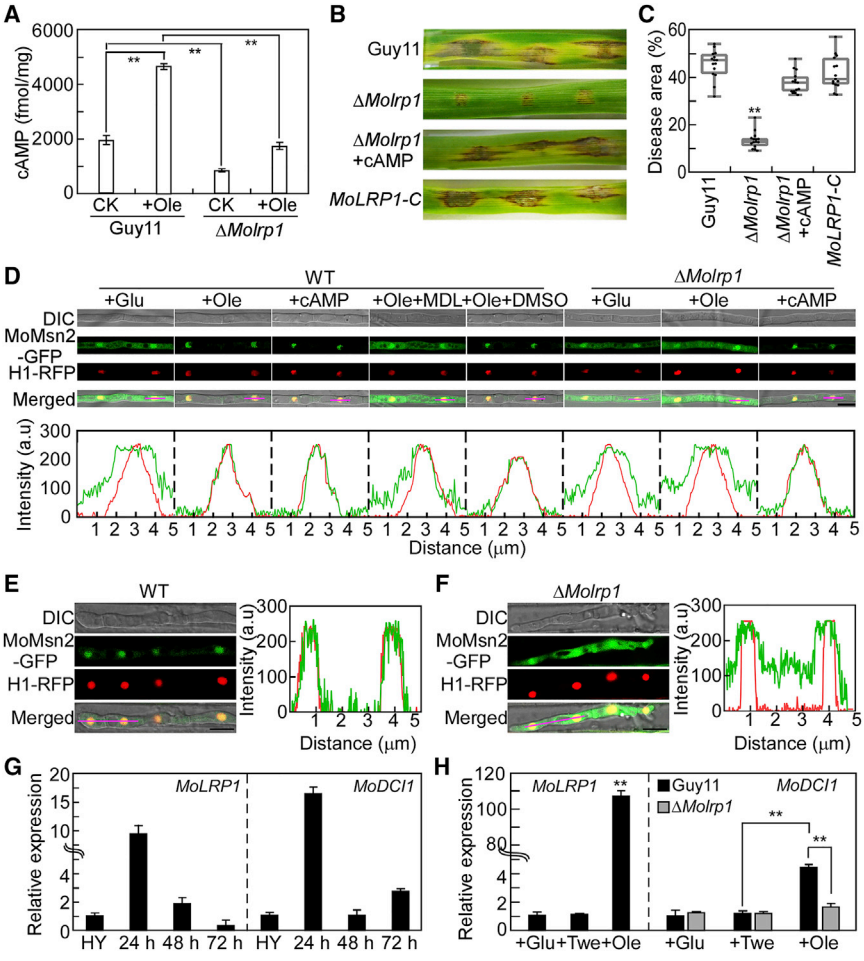

Figure 6. MoLrp1 is involved in the cAMP signaling pathway and is critical for accumulation of MoMsn2 from the cytosol to the nucleus during the early infectious stage.

(A) HPLC analysis of intracellular cAMP levels of Guy11 and Δ*Molrp1* cultured in CM with or without Ole treatment. Error bars are SDs of three biological replicates, and asterisks indicate significant differences by two-tailed Student's *t*-test at $^{**}p < 0.01$. CK, no treatment.

(B) Pathogenicity of the indicated strains on detached barley leaves with or without exogenous cAMP treatment.

(C) Statistical analysis of disease area caused by the indicated strains. Error bars are SDs of three biological replicates, and asterisks indicate significant differences by two-tailed Student's *t*-test at $^{**}p < 0.01$.

(D) Hyphae of Guy11 and Δ*Molrp1* co-expressing MoMsn2-GFP and H1-RFP proteins were observed under a confocal microscope after treatment with cAMP, Ole, or MDL-12330A (a type of adenylate cyclase inhibitor) for 10 min. Insets highlight areas analyzed by line scan. The green line represents MoMsn2-GFP; the red line represents H1-RFP. Scale bar, 10 μm.

(E and F) Conidial suspensions of Guy11 and Δ*Molrp1* co-expressing MoMsn2-GFP and H1-RFP proteins were inoculated into rice sheaths, and we observed MoMsn2-GFP accumulation in IHs at 24 hpi. Insets highlight areas analyzed by line scan. The green line represents MoMsn2-GFP; the red line represents H1-RFP. Scale bar, 20 μm.

(G) Expression profiles of *MoLRP1* and *MoDCI1* at different infectious stages. RNA was extracted from hyphae cultured for 36 h (HY) and rice leaves inoculated with wild-type conidia for 24, 48, and 72 h, respectively. Error bars are SDs of three biological replicates, and statistical analysis was performed by two-tailed Student's *t*-test.

(H) qRT–PCR analyses of the expression levels of *MoLRP1* in Guy11 and *MoDCI1* in Guy11 and Δ*Molrp1* with or without Ole treatment. Error bars are SDs of three biological replicates, and asterisks represent significant differences by two-tailed Student's *t*-test at $^{**}p < 0.01$.

MoLrp1 in the early infectious stage, thus activating expression of *MoDCI1* to promote fatty acid oxidation.

MoLrp1 and MoDci1 contribute to LD degradation during infectious growth of *M. oryzae*

Because MoLrp1, MoMsn2, and MoDci1 are important for degradation of LDs and infectious growth, we hypothesized that their proper degradation of LDs is necessary for the full virulence of *M. oryzae*. Because the Δ*Momsn2* mutant was unable to produce enough conidia for an infection assay, we examined LD accumulation in IHs of the Δ*Molrp1* and Δ*Modci1* mutants in detached rice sheaths. After 24 hpi, only a small number of LDs were observed in the wild-type Guy11, *MoLRP1-C*, and *MoDCI1-C* strains. By contrast, a large number of LDs were observed in the Δ*Molrp1* and Δ*Modci1* mutants under the same conditions. Similar results were observed in rice cells at 30 and 36 hpi (Supplemental Figure 11). These findings suggest that deletion of *MoLRP1* and *MoDCI1* impairs LD degradation in IHs of *M. oryzae*.

DISCUSSION

We previously reported that the TF MoMsn2 has a broad array of functions in development and pathogenicity through direct or indirect regulation of a series of genes in *M. oryzae* (Zhang et al., 2014; Xiao et al., 2021). Here, we demonstrated a role of MoMsn2 in fatty acid oxidation and unraveled the mechanism by which MoMsn2 accumulates from the cytosol to the nucleus upon exogenous fatty acid treatment or infection to target the fatty-acid-oxidation-related gene *MoDCI1*, thus promoting LD degradation and infectious growth of the pathogen. We further demonstrated that involvement of MoLrp1 in the regulation of the cAMP signaling pathway is important for this regulatory process. Our findings provide a link between fatty acid oxidation, cAMP signaling, and infectious growth mediated by MoMsn2 in the rice blast fungus.

Degradation of LDs contributes to energy homeostasis and cellular development in plants and yeast (Olzmann and Carvalho, 2019; Zienkiewicz and Zienkiewicz, 2020). Blocking fatty acid β-oxidation causes an abnormal accumulation of LDs (Rockenfeller and Gourlay, 2018; Jarc and Petan, 2019; Olzmann and Carvalho, 2019). Many studies have reported that strains with defects in β-oxidation and peroxisome biogenesis also showed defects in oxidation of fatty acids (Hiltunen et al., 2003; Poirier et al., 2006; Fernandez and Wilson, 2014; Aliyu et al., 2019). We demonstrated that the peroxisomal fatty acid

β-oxidation inhibitor Thi was able to inhibit oxidation of free fatty acids, degradation of LDs, and fungal invasive growth. Consistent with the role of Thi, our data showed that mutations of MoMsn2, MoLrp1, and MoDci1 produced defects in oxidation of free fatty acids, degradation of LDs, and fungal invasive growth. These results suggested that fatty acid β-oxidation was necessary for proper LD degradation and robust infection by *M. oryzae*. The physiological contribution of Dci1 to degradation of unsaturated fatty acids in yeast remains unclear (Gurvitz et al., 1999). However, overexpression of *AtDCI1,* a peroxisomal enzyme that participates in the β-oxidation cycle of unsaturated fatty acids in *Arabidopsis thaliana*, has been shown to complement the yeast Δ*Scdci1* mutant (Goepfert et al., 2005). We found that the Δ*Modci1* mutant did not grow well on Ole-supplemented medium, in contrast to results from yeast (Gurvitz et al., 1999). The Δ*Modci1* mutant also exhibited defects in peroxisome biogenesis and degradation of LDs and an altered lipid profile, implying that MoDci1 was involved in fatty acid oxidation in *M. oryzae*. In addition, we found that MoMsn2 played crucial roles in fatty acid oxidation by regulating the induction of genes involved in fatty acid β-oxidation under Ole treatment. Similar results and regulatory mechanisms have been reported in yeast (Rajvanshi et al., 2017). In contrast to the yeast TFs Msn2/Msn4, which accumulated from the cytosol to the nucleus in the presence of Ole, glycerol, and galactose, MoMsn2 appears to be involved in the response to long-chain fatty acids, but not to glycerol and galactose, in *M. oryzae*. This difference may be related to the distinct localization patterns of Msn2/Msn4 in these two organisms: yeast Msn2/Msn4 was distributed in the cytosol, whereas MoMsn2 was present in the cytosol and nucleus under normal conditions. Cytosolic MoMsn2 accumulated in the nucleus in the presence of Ole, indicating that cytosolic MoMsn2 is involved in the response to long-chain fatty acids. Because expression of *MoDCI1* did not differ markedly between Guy11 and Δ*Momsn2* under normal conditions and MoMsn2 bound to the promoter of *MoDCI1*, we speculate that although it binds to the *MoDCI1* promoter, steady-state nuclear MoMsn2 has no transcriptional activity on *MoDCI1*. Upon treatment with fatty acids, cytosolic MoMsn2 accumulates in the nucleus and activates transcription of *MoDCI1*. These cytosolic MoMsn2 proteins may undergo post-translational modification or other unknown changes that cause them to be activated during the translocation process, a possibility that remains to be studied. Overexpression of *MoDCI1* only partially restored the defects of the Δ*Momsn2* mutant, indicating that *MoDCI1* is not the only target of MoMsn2 involved in fatty acid oxidation or that only overexpression of *MoDCI1* is not sufficient for its function. Other targets of MoMsn2 must exist in *M. oryzae* to regulate fatty acid oxidation and/or other processes.

LRP1 is a multifunctional cell surface receptor that belongs to the LDLR family and has prominent functions in endocytosis, lipid metabolism, energy homeostasis, peroxisome biogenesis, cholesterol homeostasis, and signal transduction (Terrand et al., 2009; Boucher and Herz, 2011; Lin et al., 2017). Previous studies have shown that LRP1 mutation is the primary cause of hepatic insulin resistance and aortic aneurysm formation and greatly increases susceptibility to atherosclerotic lesion development (Etique et al., 2013; Ding et al., 2016; Rauch et al., 2020). In our study, MoLrp1 was found to play roles in peroxisome biogenesis, degradation of LDs, building of the lipid profile, and pathogenicity, and it was important for endocytic transport in *M. oryzae.* The localization pattern of MoLrp1 in *M. oryzae* was similar to that in mammals (Bu et al., 1994). Based on these findings, we conclude that LRP1 proteins have conserved functions, mediating endocytic transport in multiple organisms. LRP1 is required for lipolysis and stimulates fatty acid synthesis, and LRP1-deficient fibroblasts accumulate high levels of intracellular cholesterol and cholesteryl ester when stimulated for adipocyte differentiation (Terrand et al., 2009). In our study, more LDs, more free fatty acids, and more TAG were observed in the Δ*Molrp1* mutant. Lactoferrin induces lipolysis in mature adipocytes by regulating the expression levels of proteins involved in lipolysis through control of cAMP signaling pathways via LRP1 (Ikoma-Seki et al., 2015). In humans and mice, inhibition of the cAMP signaling pathway hinders cAMP synthesis and decreases lipolysis (Choi et al., 2006; Ravnskjaer et al., 2016). In our study, the cAMP level was lower in the Δ*Molrp1* mutant than in the wild type, with or without Ole. Exogenous Ole induced cAMP levels in the wild type, suggesting that Ole was able to activate intracellular cAMP levels mediated by MoLrp1. Consistent with these results, cytosolic MoMsn2 accumulated in the nucleus in the wild type upon Ole and cAMP treatment and in the Δ*Molrp1* mutant with cAMP treatment. In addition, *MoLRP1* was highly expressed during early infection and under Ole treatment, and the cytosol-to-nucleus translocation of MoMsn2 was defective in the Δ*Molrp1* mutant during the early infectious stage, indicating that MoLrp1 plays a role in regulating the function of MoMsn2 during infection. *MoDCI1* was also highly expressed during the early infectious stage and exhibited similar expression patterns in Δ*Molrp1* and Δ*Momsn2* mutants, with or without Ole treatment, indicating a regulatory relationship between MoLrp1 and MoMsn2 during fatty acid β-oxidation processes.

In conclusion, we revealed a regulatory mechanism mediated by MoMsn2 that is important for fatty acid β-oxidation in *M. oryzae*. In response to an exogenous fatty acid signal, MoMsn2 translocates from the cytosol to the nucleus, regulating expression of the fatty acid oxidation-related gene *MoDCI1* by targeting its promoter. The nuclear accumulation of MoMsn2 was induced by the cAMP signaling pathway, which was activated by the fatty acid signal. MoLrp1 likely acts as the receptor for sensing this fatty acid signal and activates the intracellular cAMP signaling pathway to induce nuclear accumulation of MoMsn2. Blocking the MoMsn2-related regulatory pathway impaired fatty acid β-oxidation, eventually resulting in accumulation of LDs and restricted infectious growth of *M. oryzae* (Figure 7). Our study provides new findings on the regulatory mechanisms of MoMsn2 during fatty acid oxidation and infectious growth of the rice blast fungus.

METHODS

Fungal strains and culture conditions

The *M. oryzae* Guy11 (ATCC201236) strain was used as the wild type throughout the study. The Δ*Momsn2* mutant and the Δ*Momsn2-C* complemented strains were generated in our previous study (Zhang et al., 2014; Xiao et al., 2021). Other strains were generated in this study. All strains were cultured on complete

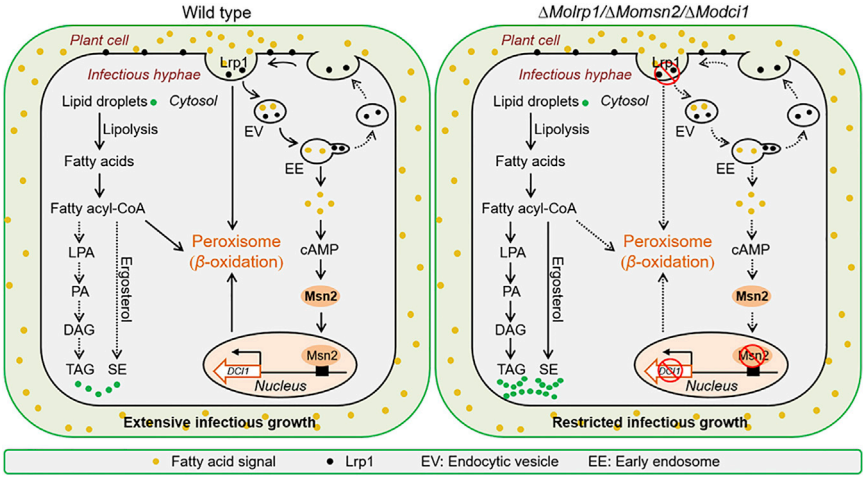

Figure 7. A proposed regulatory network mediated by MoMns2 for fatty acid β-oxidation during infectious growth of *M. oryzae*.
In response to an exogenous fatty acid signal, MoMsn2 translocates from the cytosol to the nucleus, regulating expression of the fatty acid oxidation-related gene *MoDCI1* by targeting its promoter. Nuclear accumulation of MoMsn2 is induced by the cAMP signaling pathway, which is activated by the fatty acid signal. MoLrp1 is involved in transduction of this signal through an endocytic process. Mutation of *MoMSN2*, *MoLRP1*, or *MoDCI1* in the MoMsn2-related regulatory pathway impaired fatty acid β-oxidation, eventually resulting in accumulation of LDs and restricted infectious growth of *M. oryzae*.

medium (CM) agar plates at 28°C (Zhang et al., 2010). Liquid CM medium was used to prepare the mycelia for DNA and RNA extraction as described previously (Talbot et al., 1993; Zhang et al., 2014). For the vegetative growth assay, 3 × 3-mm agar blocks were placed into CM, MM, and straw decoction and corn agar media (SDC) plates prior to incubation at 28°C (Liu et al., 2016). The colony diameter was measured 7 days after inoculation (dai). MM was supplemented with 1% (w/v) glucose, 2% (v/v) Oli, 1 mM sodium butyrate, 1 mM sodium laurate, or 1 mM sodium Ole as a sole carbon source. Because sodium Ole was dissolved in 0.03% Tween 80 (Twe; v/v), it was added to MM as a control of sodium Ole to maintain uniformity in the experiment. The relative growth rate (%) = colony diameter on fatty acid plate / colony diameter on MM plates × 100%.

Targeted gene deletion and complementation

To generate gene deletion constructs, approximately 1 kb upstream and downstream of target genes were amplified with primers (Supplemental Table 3) and ligated to the hygromycin cassette (*HPH*) released from pCX62. The resulting fragments were amplified by PCR and transformed into protoplasts of wild-type Guy11 as described previously (Zhong et al., 2016; Liu et al., 2018). To generate the complemented transformants, fragments containing the entire gene and its putative native promoter were amplified and inserted into pYF11 (bleomycin resistance) using the yeast gap repair approach (Bruno et al., 2004). The resulting constructs were sequenced and transformed into the corresponding mutants. The complemented transformants were screened by GFP signal under a fluorescence microscope.

EMSA and luciferase activity assays

The cDNA of *MoMSN2* was cloned into the pET-32a vector to heterologously express hexahistidine-tagged *MoMSN2*. MoMsn2 protein expressed in *Escherichia coli* BL21-CodonPlus (DE3) cells (Sigma-Aldrich, CMC0014) was separated and purified using Ni-nitrilotriacetic acid (Ni-NTA) agarose (QIAGEN, catalog number 30 230, Germany) according to the manufacturer's instructions. The DNA fragment of the putative gene promoter was amplified by PCR using the primers in Supplemental Table 3, mixed with the purified MoMsn2 protein, incubated for 20 min at 25°C, and then separated by agarose gel electrophoresis. Gels were visualized directly using a LI-COR Odyssey scanner (Lincoln, NE, USA) with excitation at 700 nm. For luciferase activity assays, *GFP*, *MoMSN2-GFP*, and *LUC* were inserted into the pICH86988 vector, and the promoter sequence upstream of the start codon of *MoDCI1* (1.5 kb) fused with the *LUC* gene was cloned into the pICH86900 vector. pICH86988-*LUC* containing a 35S promoter was used as a positive control, and pICH86988-GFP was used as a negative control. The resulting constructs were transformed into *Agrobacterium* GV3101 cells and then co-expressed or separately expressed in 5-week-old *N. benthamiana*. The inoculated plants were incubated for 48 h at 25°C to allow expression of transgenes. Firefly luciferase activity was analyzed using commercial dual-LUC reaction reagents (Promega, USA) according to the manufacturer's instructions and detected using a Promega GloMax Navigator microplate luminometer (Xiao et al., 2021). The luciferase chromogenic reaction assays were carried out as described previously (Huang et al., 2019).

Quantification of gene expression by qRT–PCR

Total RNA samples were extracted from mycelia, conidia, and infected rice leaves using the PureLink RNA Mini Kit (Invitrogen) according to the manufacturer's protocol. cDNA was prepared using reverse transcriptase HiScript III RT SuperMix for qPCR (Vazyme Biotech, Nanjing, China). qRT–PCR was run on an Applied Biosystems 7500 real-time PCR system (Foster City, CA, USA) with SYBR Premix ExTaq (Vazyme Biotech, Nanjing, China). The relative quantification of each transcript was calculated by the $2^{-\Delta\Delta Ct}$ method (Livak and Schmittgen, 2001) with the *M. oryzae ACTIN* gene as the internal control. For each gene, the qRT–PCR assay was repeated three times with three biological replicates. The primers used in this section are listed in Supplemental Table 3.

Conidiation, conidial germination, appressorium formation, and turgor assays

For conidiation, strains were inoculated on SDC medium, and sporulation was induced and analyzed as described previously (Zhang et al., 2010; Liu et al., 2016). Conidial germination and appressorium formation were examined on a hydrophobic surface as described previously (Zhang et al., 2011). Turgor

measurement was performed as described previously (Talbot et al., 1993; Zhang et al., 2011).

Pathogenicity assay

Rice (*Oryza sativa* cv. CO39) and barley seedlings were grown in a greenhouse at 25°C under a 12-h light/12-h dark photoperiod. Conidia were collected from 7-day-old SDC agar cultures and adjusted to 1 × 10^5 spores/ml with 0.2% (w/v) gelatin solution. Pathogenicity assays were performed as described previously (Zhang et al., 2014; Zhong et al., 2016). Diseased leaves were photographed at 5 dai (rice) or 4 dai (barley). Infectious growth was observed as described previously (Qian et al., 2021). The final concentration of Thi was 0.001 mg/ml (Sigma, T9025).

Subcellular localization, peroxisome and LD observation, and endocytosis assays

To observe the localization of MoDci1 and MoLrp1, the pYF11-*MoDCI1*-GFP construct was co-transformed into the Δ*Modci1* mutant with a type I peroxisomal targeting signal (Zhong et al., 2016). The pYF11-*MoLRP1*-GFP construct (driven by the *RP27* promoter) was co-transformed into the Δ*Molrp1* mutant with MoSft2-RFP (a Golgi marker protein) or MoLhs1-RFP (an endoplasmic reticulum marker protein) (Zhang et al., 2017, 2019). The resulting transformants were observed under a confocal fluorescence microscope (LSM 710, 63× oil, Carl Zeiss). To examine the translocation of MoMsn2 in the presence of various fatty acids or NaCl, conidia/hyphae from the strain co-expressing MoMsn2-GFP and H1-RFP were pre-treated with different fatty acids or NaCl for 30 min (conidia) or 10 min (hyphae) and observed. Fluorescence signals of MoMsn2-GFP were quantified with ImageJ and normalized with H1-RFP signals as described previously (Liu et al., 2012; McCloy et al., 2014). MDL-12330A (Sigma, M182-25MG) is a type of adenylate cyclase inhibitor (Yang et al., 2018). The final concentration of MDL-12330A (100 μM) was added to CM for vegetative growth assays. An equal concentration of DMSO was added as a control. For LD staining, vegetative hyphae cultured in liquid CM for 16 h were stained with BODIPY 493/503 (final concentration of 1 μg/ml) and incubated in the dark at 25°C for 3 min (Rajvanshi et al., 2017). Fluorescence images of peroxisomes and LDs were taken under a confocal fluorescence microscope using the 3D reconstructed confocal z stack method with 20 photos. For the endocytosis assay, conidia were stained with FM4-64 (Molecular Probes, Eugene, OR, USA) as described previously (Zhong et al., 2016; Li et al., 2017).

Intracellular cAMP and free fatty acid measurement and lipid analysis

The cAMP levels were quantified by high-performance liquid chromatography (HPLC). Intracellular cAMP extraction was performed following procedures established previously (Liu et al., 2016). For detection of free fatty acids, all of the strains were cut into 2 × 2-mm squares and cultured in liquid CM at 28°C for 36 h. The culture was then filtered to collect the mycelium and quickly ground into powder. The reaction assays were performed using the Free Fatty Acid Detection Kit (Solarbio, Beijing, China). Lipid analysis was performed as described previously (Zhao et al., 2022).

Western blot assays

Separation of nuclear and cytoplasmic proteins was performed as described previously (Lu et al., 2008; Liu et al., 2018). Conidial suspensions (20 ml) were adjusted to 5 × 10^6 spores/ml, concentrated to 1 ml by centrifugation, and then ground into powder in liquid nitrogen. For total proteins, the powder was transferred to a 2-ml tube and mixed with 1 ml lysis buffer (50 mM Tris-Cl [pH7.4], 150 mM NaCl, 2 mM EDTA, and Triton X-100). After agitating three times, supernatants were collected as total proteins by centrifugation at 10 000 *g* for 10 min at 4°C. To prepare the cytoplasmic and nuclear fractions, the powder was lysed using the Nuclear and Cytoplasmic Protein Extraction Kit (P0027, Beyotime). Protein concentration was quantified using the bicinchoninic acid (BCA) Protein Assay Kit (PC0020, Solarbio). Approximately 0.2 mg/ml of protein samples were added to Western (WES) ProteinSimple for protein analysis according to the manufacturer's instructions (Wang et al., 2017). MoMsn2-GFP and H1-RFP were detected using anti-GFP and anti-RFP, respectively. Anti-actin was used as a control. Relative GFP intensity was analyzed with ImageJ (Media Cybernetics, Shanghai, China).

Statistical analysis

For statistical analysis, mean and SD were estimated from at least three independent replicates. The significance of differences between samples was statistically evaluated using SD and ANOVA in SPSS 2.0 or GraphPad Prism 8.0.1.

SUPPLEMENTAL INFORMATION

Supplemental information is available at *Plant Communications Online*.

FUNDING

This work was supported by grants from the Natural Science Foundation of China (31871912 and 32061143045 to H.Z.) and the Fundamental Research Funds for the Central Universities (KYZ201816 to H.Z.).

AUTHOR CONTRIBUTIONS

H.Z., Z.Z., X.Z., and T.Z. designed the experiments. T.Z., X.W., X.L., Y.-N.L., Y.L., S.W., L.X., R.Z., J.Y., G.L., and X.L. conducted the experiments. H.Z. and T.Z. wrote the manuscript.

ACKNOWLEDGMENTS

We thank Prof. Gang Li at Nanjing Agricultural University for critical reading of this work. No conflict of interest is declared.

Received: July 24, 2022
Revised: January 5, 2023
Accepted: February 8, 2023
Published: February 11, 2023

REFERENCES

Abdul, W., Aliyu, S.R., Lin, L., Sekete, M., Chen, X., Otieno, F.J., Yang, T., Lin, Y., Norvienyeku, J., and Wang, Z. (2018). Family-four aldehyde dehydrogenases play an indispensable role in the pathogenesis of *Magnaporthe oryzae*. Front. Plant Sci. **9**:1–12.

Aliyu, S.R., Lin, L., Chen, X., Abdul, W., Lin, Y., Otieno, F.J., Shabbir, A., Batool, W., Zhang, Y., Tang, W., et al. (2019). Disruption of putative short-chain acyl-CoA dehydrogenases compromised free radical scavenging, conidiogenesis, and pathogenesis of *Magnaporthe oryzae*. Fungal Genet. Biol. **127**:23–34.

Boucher, P., and Herz, J. (2011). Signaling through LRP1: protection from atherosclerosis and beyond. Biochem. Pharmacol. **81**:1–5.

Brasaemle, D.L., Subramanian, V., Garcia, A., Marcinkiewicz, A., and Rothenberg, A. (2009). Perilipin A and the control of triacylglycerol metabolism. Mol. Cell. Biochem. **326**:15–21.

Bruno, K.S., Tenjo, F., Li, L., Hamer, J.E., and Xu, J.R. (2004). Cellular localization and role of kinase activity of *PMK1* in *Magnaporthe grisea*. Eukaryot. Cell **3**:1525–1532.

Bu, G., Maksymovitch, E.A., Geuze, H., and Schwartz, A.L. (1994). Subcellular localization and endocytic function of low density lipoprotein receptor-related protein in human glioblastoma cells. J. Biol. Chem. **269**:29874–29882.

Chang, W., Zhang, M., Zheng, S., Li, Y., Li, X., Li, W., Li, G., Lin, Z., Xie, Z., Zhao, Z., and Lou, H. (2015). Trapping toxins within lipid droplets is a resistance mechanism in fungi. Sci. Rep. **5**:15133.

Choi, Y.H., Park, S., Hockman, S., Zmuda-Trzebiatowska, E., Svennelid, F., Haluzik, M., Gavrilova, O., Ahmad, F., Pepin, L., Napolitano, M., et al. (2006). Alterations in regulation of energy homeostasis in cyclic nucleotide phosphodiesterase 3B-null mice. J. Clin. Invest. **116**:3240–3251.

Deng, S., Gu, Z., Yang, N., Li, L., Yue, X., Que, Y., Sun, G., Wang, Z., and Wang, J. (2016). Identification and characterization of the peroxin 1 gene *MoPEX1* required for infection-related morphogenesis and pathogenicity in *Magnaporthe oryzae*. Sci. Rep. **6**:36292–36313.

Ding, Y., Xian, X., Holland, W.L., Tsai, S., and Herz, J. (2016). Low-density lipoprotein receptor-related protein-1 protects against hepatic Insulin resistance and hepatic steatosis. EBioMedicine **7**:135–145.

Duncan, R.E., Ahmadian, M., Jaworski, K., Sarkadi-Nagy, E., and Sul, H.S. (2007). Regulation of lipolysis in adipocytes. Annu. Rev. Nutr. **27**:79–101.

Etique, N., Verzeaux, L., Dedieu, S., and Emonard, H. (2013). LRP-1: a checkpoint for the extracellular matrix proteolysis. BioMed Res. Int. **2013**:152–163.

Fatima, U., and Senthil-Kumar, M. (2015). Plant and pathogen nutrient acquisition strategies. Front. Plant Sci. **6**:750.

Fernandez, J., and Wilson, R.A. (2014). Cells in cells: morphogenetic and metabolic strategies conditioning rice infection by the blast fungus *Magnaporthe oryzae*. Protoplasma **251**:37–47.

Fernandez, J., Wright, J.D., Hartline, D., Quispe, C.F., Madayiputhiya, N., and Wilson, R.A. (2012). Principles of carbon catabolite repression in the rice blast fungus: Tps1, Nmr1-3, and a MATE-family pump regulate glucose metabolism during infection. PLoS Genet. **8**:e1002673.

Fu, Y., Chen, N., Wang, Z., Luo, S., Ding, Y., and Lu, B. (2021). Degradation of lipid droplets by chimeric autophagy-tethering compounds. Cell Res. **31**:965–979.

Goepfert, S., Vidoudez, C., Rezzonico, E., Hiltunen, J.K., and Poirier, Y. (2005). Molecular identification and characterization of the Arabidopsis delta(3,5),delta(2,4)-dienoyl-coenzyme A isomerase, a peroxisomal enzyme participating in the beta-oxidation cycle of unsaturated fatty acids. Plant Physiol. **138**:1947–1956.

Goh, J., Jeon, J., Kim, K.S., Park, J., Park, S.Y., and Lee, Y.H. (2011). The *PEX7*-mediated peroxisomal import system is required for fungal development and pathogenicity in *Magnaporthe oryzae*. PLoS One **6**:e28220.

Graef, M. (2018). Lipid droplet-mediated lipid and protein homeostasis in budding yeast. FEBS Lett. **592**:1291–1303.

Greenberg, A.S., Coleman, R.A., Kraemer, F.B., McManaman, J.L., Obin, M.S., Puri, V., Yan, Q.W., Miyoshi, H., and Mashek, D.G. (2011). The role of lipid droplets in metabolic disease in rodents and humans. J. Clin. Invest. **121**:2102–2110.

Gurvitz, A., Mursula, A.M., Yagi, A.I., Hartig, A., Ruis, H., Rottensteiner, H., and Hiltunen, J.K. (1999). Alternatives to the isomerase-dependent pathway for the beta-oxidation of oleic acid are dispensable in *Saccharomyces cerevisiae*: identification of YOR180c/DCI1 encoding peroxisomal delta(3,5)-delta(2,4)-dienoyl-CoA isomerase. J. Biol. Chem. **274**:24514–24521.

Hiltunen, J.K., Mursula, A.M., Rottensteiner, H., Wierenga, R.K., Kastaniotis, A.J., and Gurvitz, A. (2003). The biochemistry of peroxisomal β-oxidation in the yeast *Saccharomyces cerevisiae*. FEMS Microbiol. Rev. **27**:35–64.

Huang, J., Chen, L., Lu, X., Peng, Q., Zhang, Y., Yang, J., Zhang, B.Y., Yang, B., Waletich, J.R., Yin, W., et al. (2019). Natural allelic variations provide insights into host adaptation of *Phytophthora* avirulence effector PsAvr3c. New Phytol. **221**:1010–1022.

Ikoma-Seki, K., Nakamura, K., Morishita, S., Ono, T., Sugiyama, K., Nishino, H., Hirano, H., and Murakoshi, M. (2015). Role of *LRP1* and *ERK* and cAMP signaling pathways in lactoferrin-induced lipolysis in mature rat adipocytes. PLoS One **10**:e0141378.

Jarc, E., and Petan, T. (2019). Lipid droplets and the management of cellular stress. Yale J. Biol. Med. **92**:435–452.

Kohlwein, S.D., Veenhuis, M., and van der Klei, I.J. (2013). Lipid droplets and peroxisomes: key players in cellular lipid homeostasis or a matter of fat–store 'em up or burn 'em down. Genetics **193**:1–50.

Li, X., Gao, C., Li, L., Liu, M., Yin, Z., Zhang, H., Zheng, X., Wang, P., and Zhang, Z. (2017). MoEnd3 regulates appressorium formation and virulence through mediating endocytosis in rice blast fungus *Magnaporthe oryzae*. PLoS Pathog. **13**:e1006449.

Lin, J.P., Mironova, Y.A., Shrager, P., and Giger, R.J. (2017). LRP1 regulates peroxisome biogenesis and cholesterol homeostasis in oligodendrocytes and is required for proper CNS myelin development and repair. Elife **6**:30498.

Liu, N., Yun, Y., Yin, Y., Hahn, M., Ma, Z., and Chen, Y. (2019). Lipid droplet biogenesis regulated by the FgNem1/Spo7-FgPah1 phosphatase cascade plays critical roles in fungal development and virulence in *Fusarium graminearum*. New Phytol. **223**:412–429.

Liu, Q., Liu, S., Kodama, L., Driscoll, M.R., and Wu, M.N. (2012). Two dopaminergic neurons signal to the dorsal fan-shaped body to promote wakefulness in *Drosophila*. Curr. Biol. **22**:2114–2123.

Liu, X., Qian, B., Gao, C., Huang, S., Cai, Y., Zhang, H., Zheng, X., Wang, P., and Zhang, Z. (2016). The putative protein phosphatase MoYvh1 functions upstream of MoPdeH to regulate the development and pathogenicity in *Magnaporthe oryzae*. Mol. Plant Microbe Interact. **29**:496–507.

Liu, X., Yang, J., Qian, B., Cai, Y., Zou, X., Zhang, H., Zheng, X., Wang, P., and Zhang, Z. (2018). MoYvh1 subverts rice defense through functions of ribosomal protein MoMrt4 in *Magnaporthe oryzae*. PLoS Pathog. **14**:e1007016.

Livak, K.J., and Schmittgen, T.D. (2001). Analysis of relative gene expression data using real-time quantitative PCR and the 2(-Delta Delta C(T)) Method. Methods **25**:402–408.

Lu, J., Zhang, F., Zhao, D., Hong, L., Min, J., Zhang, L., Li, F., Yan, Y., Li, H., Ma, Y., and Li, Q. (2008). ATRA-inhibited proliferation in glioma cells is associated with subcellular redistribution of beta-catenin via up-regulation of Axin. J. Neuro Oncol. **87**:271–277.

McCloy, R.A., Rogers, S., Caldon, C.E., Lorca, T., Castro, A., and Burgess, A. (2014). Partial inhibition of Cdk1 in G(2) phase overrides the SAC and decouples mitotic events. Cell Cycle **13**:1400–1412.

Monson, E.A., Trenerry, A.M., Laws, J.L., Mackenzie, J.M., and Helbig, K.J. (2021). Lipid droplets and lipid mediators in viral infection and immunity. FEMS Microbiol. Rev. **45**. fuaa066–20.

Olzmann, J.A., and Carvalho, P. (2019). Dynamics and functions of lipid droplets. Nat. Rev. Mol. Cell Biol. **20**:137–155.

Pagnon, J., Matzaris, M., Stark, R., Meex, R.C.R., Macaulay, S.L., Brown, W., O'Brien, P.E., Tiganis, T., and Watt, M.J. (2012).

Identification and functional characterization of protein kinase A phosphorylation sites in the major lipolytic protein, adipose triglyceride lipase. Endocrinology **153**:4278–4289.

Patkar, R.N., Ramos-Pamplona, M., Gupta, A.P., Fan, Y., and Naqvi, N.I. (2012). Mitochondrial beta-oxidation regulates organellar integrity and is necessary for conidial germination and invasive growth in *Magnaporthe oryzae*. Mol. Microbiol. **86**:1345–1363.

Petan, T., Jarc, E., and Jusović, M. (2018). Lipid droplets in cancer: guardians of fat in a stressful world. Molecules **23**:1941.

Poirier, Y., Antonenkov, V.D., Glumoff, T., and Hiltunen, J.K. (2006). Peroxisomal beta-oxidation-a metabolic pathway with multiple functions. Biochim. Biophys. Acta **1763**:1413–1426.

Qian, B., Liu, X., Ye, Z., Zhou, Q., Liu, P., Yin, Z., Wang, W., Zheng, X., Zhang, H., and Zhang, Z. (2021). Phosphatase-associated protein MoTip41 interacts with the phosphatase MoPpe1 to mediate crosstalk between TOR and cell wall integrity signalling during infection by the rice blast fungus *Magnaporthe oryzae*. Environ. Microbiol. **23**:791–809.

Rajvanshi, P.K., Arya, M., and Rajasekharan, R. (2017). The stress-regulatory transcription factors Msn2 and Msn4 regulate fatty acid oxidation in budding yeast. J. Biol. Chem. **292**:18628–18643.

Rauch, J.N., Luna, G., Guzman, E., Audouard, M., Challis, C., Sibih, Y.E., Leshuk, C., Hernandez, I., Wegmann, S., Hyman, B.T., et al. (2020). LRP1 is a master regulator of tau uptake and spread. Nature **580**:381–385.

Ravnskjaer, K., Madiraju, A., and Montminy, M. (2016). Role of the cAMP pathway in glucose and lipid metabolism. Handb. Exp. Pharmacol. **233**:29–49.

Rejman, J., Bragonzi, A., and Conese, M. (2005). Role of clathrin- and caveolae-mediated endocytosis in gene transfer mediated by lipo- and polyplexes. Mol. Ther. **12**:468–474.

Ren, Y., and Schulz, H. (2003). Metabolic functions of the two pathways of oleate beta-oxidation double bond metabolism during the beta-oxidation of oleic acid in rat heart mitochondria. J. Biol. Chem. **278**:111–116.

Rockenfeller, P., and Gourlay, C.W. (2018). Lipotoxicty in yeast: a focus on plasma membrane signalling and membrane contact sites. FEMS Yeast Res. **18**. foy034–8.

Rockenfeller, P., Smolnig, M., Diessl, J., Bashir, M., Schmiedhofer, V., Knittelfelder, O., Ring, J., Franz, J., Foessl, I., Khan, M.J., et al. (2018). Diacylglycerol triggers Rim101 pathway-dependent necrosis in yeast: a model for lipotoxicity. Cell Death Differ. **25**:767–783.

Shen, S., Faouzi, S., Souquere, S., Roy, S., Routier, E., Libenciuc, C., André, F., Pierron, G., Scoazec, J.Y., and Robert, C. (2020). Melanoma persister cells are tolerant to *BRAF/MEK* inhibitors via *ACOX1*-mediated fatty acid oxidation. Cell Rep. **33**:108421.

Shepherd, R.E., Noble, E.G., Klug, G.A., and Gollnick, P.D. (1981). Lipolysis and cAMP accumulation in adipocytes in response to physical training. J. Appl. Physiol. Respir. Environ. Exerc. Physiol. **50**:143–148.

Talbot, N.J., Ebbole, D.J., and Hamer, J.E. (1993). Ldentification and characterization of *MPGI*, a gene involved in pathogenicity from the rice blast fungus *Magnaporthe grisea*. Plant Cell **5**:1575–2159.

Terrand, J., Bruban, V., Zhou, L., Gong, W., El Asmar, Z., May, P., Zurhove, K., Haffner, P., Philippe, C., Woldt, E., et al. (2009). LRP1 controls intracellular cholesterol storage and fatty acid synthesis through modulation of Wnt signaling. J. Biol. Chem. **284**:381–388.

Walther, T.C., and Farese, R.V., Jr. (2012). Lipid droplets and cellular lipid metabolism. Annu. Rev. Biochem. **81**:687–714.

Wang, J., Valdez, A., and Chen, Y. (2017). Evaluation of automated Wes system as an analytical and characterization tool to support monoclonal antibody drug product development. J. Pharm. Biomed. Anal. **139**:263–268.

Wang, J., Li, L., Zhang, Z., Qiu, H., Li, D., Fang, Y., Jiang, H., Chai, R.Y., Mao, X., Wang, Y., and Sun, G. (2015). One of three Pex11 family members is required for peroxisomal proliferation and full virulence of the rice blast fungus *Magnaporthe oryzae*. PLoS One **10**. 101342499-21.

Wang, Z.Y., Soanes, D.M., Kershaw, M.J., and Talbot, N.J. (2007). Functional analysis of lipid metabolism in *Magnaporthe grisea* reveals a requirement for peroxisomal fatty acid beta-oxidation during appressorium-mediated plant infection. Mol. Plant Microbe Interact. **20**:475–491.

Willnow, T.E., Nykjaer, A., and Herz, J. (1999). Lipoprotein receptors: new roles for ancient proteins. Nat. Cell Biol. **1**:157–162.

Wu, X., Geng, F., Cheng, X., Guo, Q., Zhong, Y., Cloughesy, T.F., Yong, W.H., Chakravarti, A., and Guo, D. (2020). Lipid droplets maintain energy homeostasis and glioblastoma growth via autophagic release of stored fatty acids. iScience **23**:101569.

Xiao, Y., Liu, L., Zhang, T., Zhou, R., Ren, Y., Li, X., Shu, H., Ye, W., Zheng, X., Zhang, Z., and Zhang, H. (2021). Transcription factor MoMsn2 targets the putative 3-methylglutaconyl-CoA hydratase-encoding gene *MoAUH1* to govern infectious growth via mitochondrial fusion/fission balance in *Magnaporthe oryzae*. Environ. Microbiol. **23**:774–790.

Yang, L.N., Yin, Z., Zhang, X., Feng, W., Xiao, Y., Zhang, H., Zheng, X., and Zhang, Z. (2018). New findings on phosphodiesterases, MoPdeH and MoPdeL, in *Magnaporthe oryzae* revealed by structural analysis. Mol. Plant Pathol. **19**:1061–1074.

Zhang, H., Liu, K., Zhang, X., Song, W., Zhao, Q., Dong, Y., Guo, M., Zheng, X., and Zhang, Z. (2010). A two-component histidine kinase, *MoSLN1*, is required for cell wall integrity and pathogenicity of the rice blast fungus, *Magnaporthe oryzae*. Curr. Genet. **56**:517–528.

Zhang, H., Tang, W., Liu, K., Huang, Q., Zhang, X., Yan, X., Chen, Y., Wang, J., Qi, Z., Wang, Z., et al. (2011). Eight RGS and RGS-like proteins orchestrate growth, differentiation, and pathogenicity of *Magnaporthe oryzae*. PLoS Pathog. **7**:e1002450.

Zhang, H., Zhao, Q., Guo, X., Guo, M., Qi, Z., Tang, W., Dong, Y., Ye, W., Zheng, X., Wang, P., and Zhang, Z. (2014). Pleiotropic function of the putative zinc-finger protein MoMsn2 in *Magnaporthe oryzae*. Mol. Plant Microbe Interact. **27**:446–460.

Zhang, S., Liu, X., Li, L., Yu, R., He, J., Zhang, H., Zheng, X., Wang, P., and Zhang, Z. (2017). The ArfGAP protein MoGlo3 regulates the development and pathogenicity of *Magnaporthe oryzae*. Environ. Microbiol. **19**:3982–3996.

Zhang, S., Yang, L., Li, L., Zhong, K., Wang, W., Liu, M., Li, Y., Liu, X., Yu, R., He, J., et al. (2019). System-wide characterization of MoArf GTPase family proteins and adaptor protein MoGga1 involved in the development and pathogenicity of *Magnaporthe oryzae*. mBio **10**. e02398-02319.

Zhao, J., Sun, P., Sun, Q., Li, R., Qin, Z., Sha, G., Zhou, Y., Bi, R., Zhang, H., Zheng, L., et al. (2022). The MoPah1 phosphatidate phosphatase is involved in lipid metabolism, development, and pathogenesis in *Magnaporthe oryzae*. Mol. Plant Pathol. **23**:720–732.

Zhong, K., Li, X., Le, X., Kong, X., Zhang, H., Zheng, X., Wang, P., and Zhang, Z. (2016). MoDnm1 dynamin mediating peroxisomal and mitochondrial fission in complex with MoFis1 and MoMdv1 is important for development of functional appressorium in *Magnaporthe oryzae*. PLoS Pathog. **12**:e1005823.

Zienkiewicz, K., and Zienkiewicz, A. (2020). Degradation of lipid droplets in plants and algae-right time, many paths, one goal. Front. Plant Sci. **11**:579019.